Hindawi
Advances in Civil Engineering
Volume 2019, Article ID 8130240, 12 pages
https://doi.org/10.1155/2019/8130240

Research Article

Safety Prediction Using Vehicle Safety Evaluation Model Passing on Long-Span Bridge with Fully Connected Neural Network

Yang Yang[1,2], **Lin Yang**[1,2], **Bo Wu**[1,2], **Gang Yao**[1,2], **Hang Li**[1,2] and **Soltys Robert**[3]

[1]*Key Laboratory of New Technology for Construction of Cities in Mountain Area, Ministry of Education, Chongqing, China*
[2]*School of Civil Engineering, Chongqing University, Chongqing, China*
[3]*Technical University of Kosice, Kosice, Slovakia*

Correspondence should be addressed to Yang Yang; yy20052710@163.com and Gang Yao; yaocqu@vip.sina.com

Received 2 July 2019; Accepted 12 September 2019; Published 15 October 2019

Academic Editor: Yinshan Tang

The safety condition of vehicles passing on long-span bridges has attracted more and more attention in recent years. Many research studies have been done to find convenience and efficiency measures. A vehicle safety evaluation model passing on a long-span bridge is presented in this paper based on fully connected neural network (FCN). The first step is to investigate the long-span bridge responses with wind excitation by using the wind tunnel test and finite element model. Subsequently, typical vehicle models are given and a vehicle-bridge system is established by considering weather conditions. Accident types of vehicles with severe weather are estimated. In particular, the input and output variables of the vehicle safety evaluation model are determined, and simultaneously training, validation, and testing data are achieved. Twenty-nine models have been compared and analyzed by using hidden layer, initial learning rate, batch size, activation function, and optimization method. It is found that the 4-15-15-4 model occupies a preferable prediction performance, and it can provide a kind of utility for traffic control and reduce the probability of vehicle accidents on the bridge.

1. Introduction

Long-span bridges often play a significant role in regional traffic. The complex interaction in the vehicle-bridge system directly affects safety of traffic on these long-span bridges. This problem has attracted many attentions in the field of bridge [1]. Most of the research in the vehicle-bridge system is aimed at two aspects. On the one hand, the vehicle-bridge dynamic coupling system effects bridge vibration subjected to cyclic loadings due to the coupled vibration excited by vehicles, with considering severe weather [2–8]. On the other hand, it effects vehicle vibration, including comfort ability for the driver. Meanwhile, the vehicle's safety is highly concerned [9–12]. Driving speed limits of bridges and decisions on closing of the traffic on bridges are mainly decided according to experience. Closing the traffic frequently will totally affect the traffic flow in the transportation line. And hence, it is important to set the traveling speed limit or to make operational decisions for severe weather.

Numerous studies have shown that the evaluation of the vehicle-bridge system is a difficult task. Theoretical derivations of the vehicle-bridge system motion equation mainly include the iterative method and the coupled method [13–19]. The iterative method solves two sets of motion equations, respectively, including the vehicle motion equation and bridge motion equation. Displacement compatibility and force equilibrium conditions are transmitted by the roughness of the bridge deck. In the coupled method, the bridge is modeled as a grillage beam system, and the vehicle is idealized as a multiaxle sprung load with different degrees of freedom moving across rough bridge decks. The vehicle motion equation and bridge motion equation are resulted in a single matrix for the mass, damping, and stiffness of the vehicle-bridge system. The derived motion

equations of the coupled vehicle-bridge system are then solved by the direct integration method. With the development of computers, the finite element method (FEM) and component element method (CEM) are used in the vibration problem of the vehicle-bridge system [20–23]. Based on previous studies, effects of excitation are researched, including seismic excitation, wind excitation, rain excitation, roughness excitation, and traffic flow excitation. The wind excitation is most widely concerned [24–33]. Dynamic analysis of the vehicle-bridge system is maturing, with a wealth of well-understood methods and algorithms, particularly in the wind-vehicle-bridge system.

Vehicle-bridge systems are relatively difficult to calculate; meanwhile, extraction processes of bridge response and vibration of vehicles are relatively complicated. Although accurate results can be derived from the existing methods, a variety of working condition calculations may be required which take much time and effort. Some scholars have applied the neural network principle to the response prediction of the vehicle-bridge system which can improve the computational efficiency [34, 35].

The research on the vehicle-bridge system with severe weather can be potentially applied into practical engineering, particularly in vehicle accident issue prediction. This paper focuses on developing a neural network model to predict safety of vehicles passing on the bridge by considering the effect of severe weather. It could provide a comprehensive review of overall performance of the vehicle-bridge system with severe weather, including interaction of the bridge and vehicles. The research achievement can apply the analysis result of the vehicle-bridge dynamic coupled system into practical engineering conveniently and efficiently.

2. Establishment of Vehicle-Bridge System

Safety of the vehicle-bridge system is affected by many factors. Researchers quantified the most important factors in the vehicle-bridge system in the safety evaluation. Effect of the bridge is considered by the acting force on vehicle, and then the safety evaluation model of the vehicle-bridge system is established by considering the vehicle type, vehicle speed, wind velocity, and weather condition.

2.1. Bridge Model. *Cuntan Yangtze Bridge* is taken as the project background. Detail dimensions of the bridge section are shown in Figure 1.

In order to get the static force coefficients, the bridge section model is used in the wind tunnel test. Aerostatic coefficients are tested by the subsection elastic model in the wind tunnel, which are used to calculate aerostatic load. The subsection elastic model is made of wood. Pedestrian guardrails, anticollision guardrails, and center separation band guardrails are manufactured with plastic plates by machine. The subsection elastic model has a scalar of 1/60 to the real bridge section, and parameters are given in Table 1. The aerostatic effects on the bridge deck are measured by aerostatic force experimental coefficients. Figure 2 shows the aerostatic force experimental in the wind tunnel test. The results of aerostatic force coefficients at different wind attack angles are shown in Figure 3. C_{L}, $C_{\mathrm{D},}$ and C_{M} are dimensionless lift, drag, and moment coefficients, and C'_{L}, C'_{D}, and C'_{M} are derivatives of lift, drag, and moment coefficients.

Aerostatic force coefficients and their derivatives are used to calculate the buffeting loads. Buffeting loads at per unit span length are expressed in the following equations:

$$L_b(t) = \frac{1}{2}\rho U^2 qB\left[2C_{\mathrm{L}}(\theta)\chi_{Lu}\frac{u(t)}{U} + \left(C'_{\mathrm{L}}(\theta)\right) + \left(C_{\mathrm{D}}(\theta)\right)\chi_{Lu}\frac{w(t)}{U}\right], \tag{1}$$

$$D_b(t) = \frac{1}{2}\rho U^2 B\left[2C_{\mathrm{L}}(\theta)\chi_{Lu}\frac{u(t)}{U} + \left(C'_{\mathrm{D}}(\theta)\right)\chi_{Dw}\frac{w(t)}{U}\right], \tag{2}$$

$$M_b(t) = \frac{1}{2}\rho U^2 B^2\left[2C_{\mathrm{M}}(\theta)\chi_{Lu}\frac{u(t)}{U} + \left(C'_{\mathrm{M}}(\theta)\right)\chi_{Mw}\frac{w(t)}{U}\right], \tag{3}$$

where L_b, D_b, and M_b represent the lift, drag, and moment due to buffeting effects, respectively; $C_{\mathrm{L}}(\theta)$, $C_{\mathrm{D}}(\theta)$, and $C_{\mathrm{M}}(\theta)$ are dimensionless lift, drag, and moment coefficients at a specified wind angle; $C'_{\mathrm{L}} = \mathrm{d}C_{\mathrm{L}}/\mathrm{d}\theta$, $C'_{\mathrm{D}} = \mathrm{d}C_{\mathrm{D}}/\mathrm{d}\theta$, and $C'_{\mathrm{M}} = \mathrm{d}C_{\mathrm{M}}/\mathrm{d}\theta$ are the deviates of aerostatic forces; $u(t)$ and $w(t)$ are wind velocity fluctuations in the horizontal and vertical directions, respectively; and χ_{Lu}, χ_{Du}, and χ_{Mu} are aerodynamic admittance.

Buffeting loads can be expressed in the following equations [36–38]:

$$L(t) = L_{\mathrm{se}}(t) + L_b(t), \tag{4}$$

$$D(t) = D_{\mathrm{se}}(t) + D_b(t), \tag{5}$$

$$M(t) = M_{\mathrm{se}}(t) + M_b(t), \tag{6}$$

where L_{se}, $D_{\mathrm{se},}$ and M_{se} represent the lift, drag, and moment due to self-excited motions, respectively. Self-excited and buffeting forces are shown schematically in Figure 4.

The lift, drag, and moment of the self-excited part of the force at per unit length of the deck can be expressed in the following equations:

$$L_{\mathrm{se}}(t) = \frac{1}{2}\rho U^2 B\left[KH_1^*\frac{\dot{h}}{U} + KH_2^*\frac{B\dot{\alpha}}{U} + K^2H_3^*\alpha\right], \tag{7}$$

$$D_{\mathrm{se}}(t) = \frac{1}{2}\rho U^2 B\left[KH_4^*\frac{\dot{h}}{U} + KH_5^*\frac{B\dot{\alpha}}{U} + K^2H_6^*\alpha\right], \tag{8}$$

$$M_{\mathrm{se}}(t) = \frac{1}{2}\rho U^2 B\left[KH_7^*\frac{\dot{h}}{U} + KH_8^*\frac{B\dot{\alpha}}{U} + K^2H_9^*\alpha\right], \tag{9}$$

where ρ represents the density of air, B represents the width of the bridge deck, K represents the reduced frequency and $K = B\omega/U$, ω represents the circular frequency of the bridge motion, H_i^* $(i = 1, 2, 3, \ldots, 9)$ represent flutter derivatives of

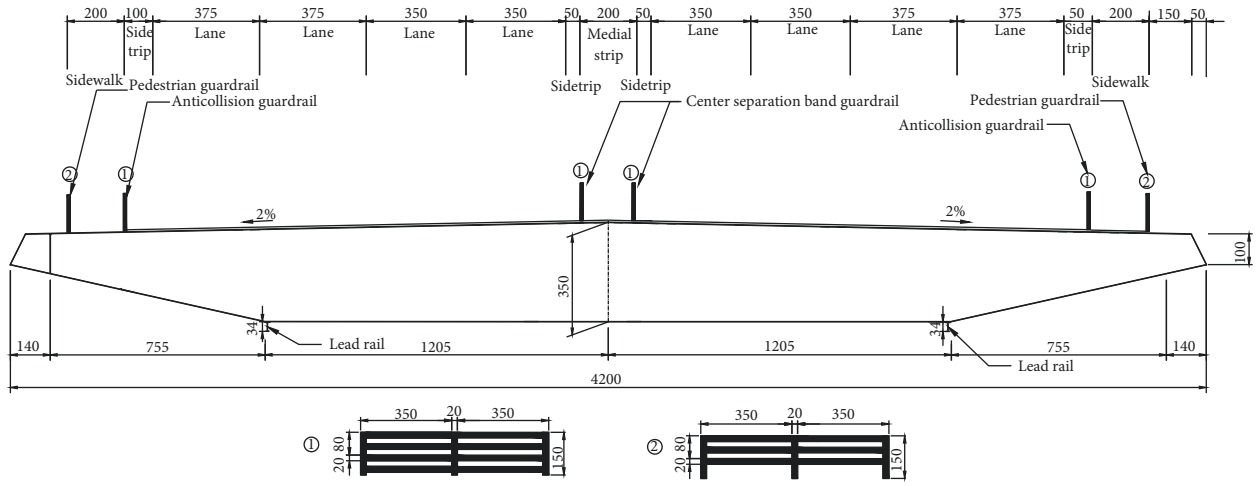

Figure 1: Dimensions of standard cross section (unit: cm).

Table 1: Design parameters of the section elastic model.

Parameter	Unit	Actual value	Required value	Value in test
Height	m	3.5	0.0583	0.0583
Width	m	42.0	0.7	0.7
Linear mass	kg/m	27600	7.667	7.667
Linear mass moment of inertia	Kg·m^2/m	5137700	0.3987	0.3987
Vertical bending frequency	Hz	0.17446	2.216	2.216
Vertical bending damping ratio	%	0.5	0.389	0.372
Torsion frequency	Hz	0.39726	5.404	5.404
Torsion damping ratio	%	0.5	0.439	0.422

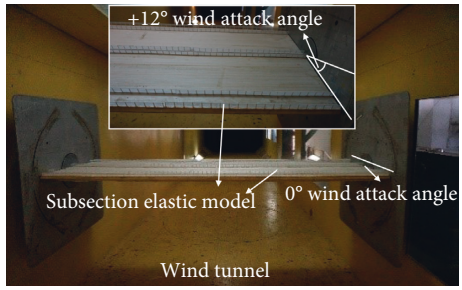

Figure 2: Test of aerostatic force coefficients.

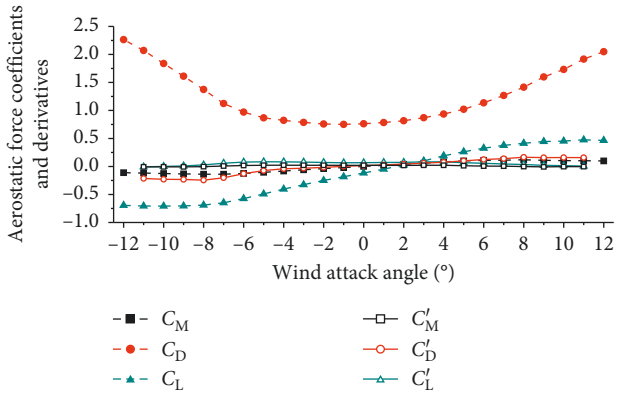

Figure 3: Aerostatic force coefficients and their derivatives.

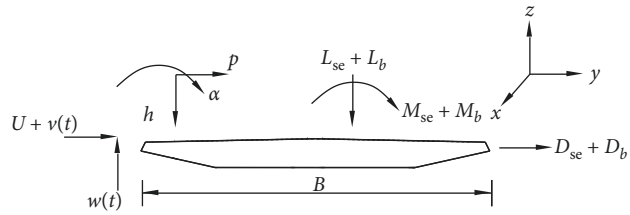

Figure 4: Aerodynamic forces on the bridge deck.

the bridge deck measured through the wind tunnel tests, U represents the mean wind velocity, and h and α represent the vertical and rotational displacement of the bridge deck, respectively.

The finite element of the bridge has been established and accuracy of the model has been proved by authors in [36, 37]. The finite element model is used to calculate the bridge accelerations with different wind velocities. Accelerations in the middle of the bridge girder at 5.0 m/s are given in Figure 5. Power density spectrums in the middle of the bridge girder at 5.0 m/s are given in Figure 6. Accelerations along the main girder at different wind velocities are given in Figure 7.

Accelerations shown in Figure 5 are taken as apply force bridge passing to the vehicle. Accelerations in vertical and transverse directions are taken to analyze in the frequency domain. And hence, the power density spectrums are given in Figure 6. The abscissa is the linear coordinate, and the

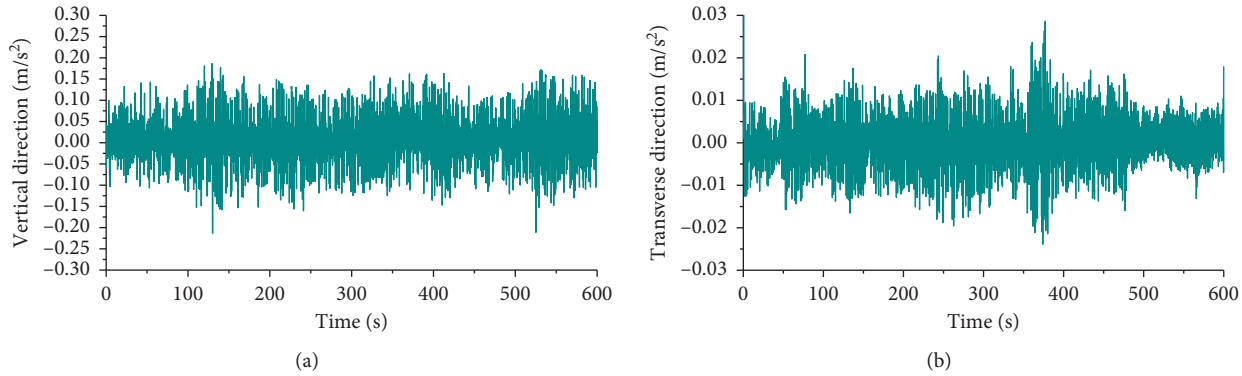

Figure 5: Acceleration in the middle of the bridge girder at 5.0 m/s: (a) vertical and (b) transverse.

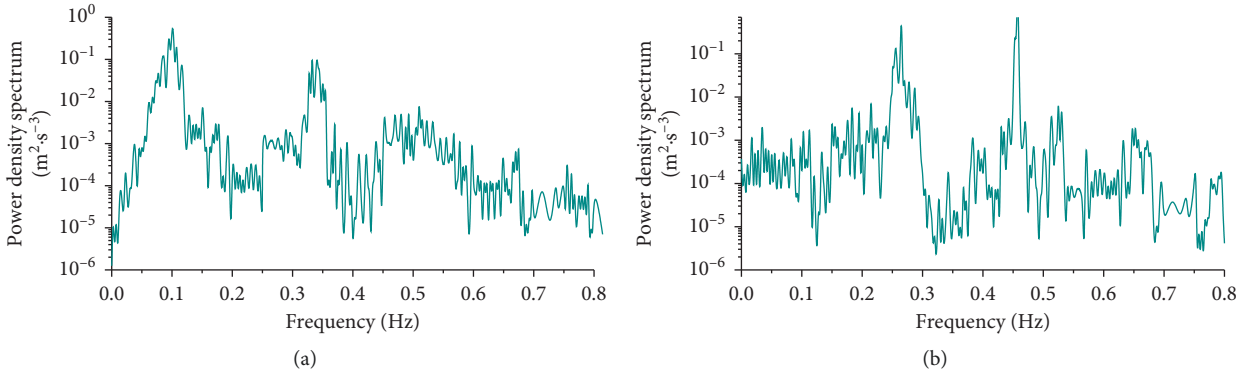

Figure 6: Power density spectrum in the middle of the bridge girder at 5.0 m/s: (a) vertical and (b) transverse.

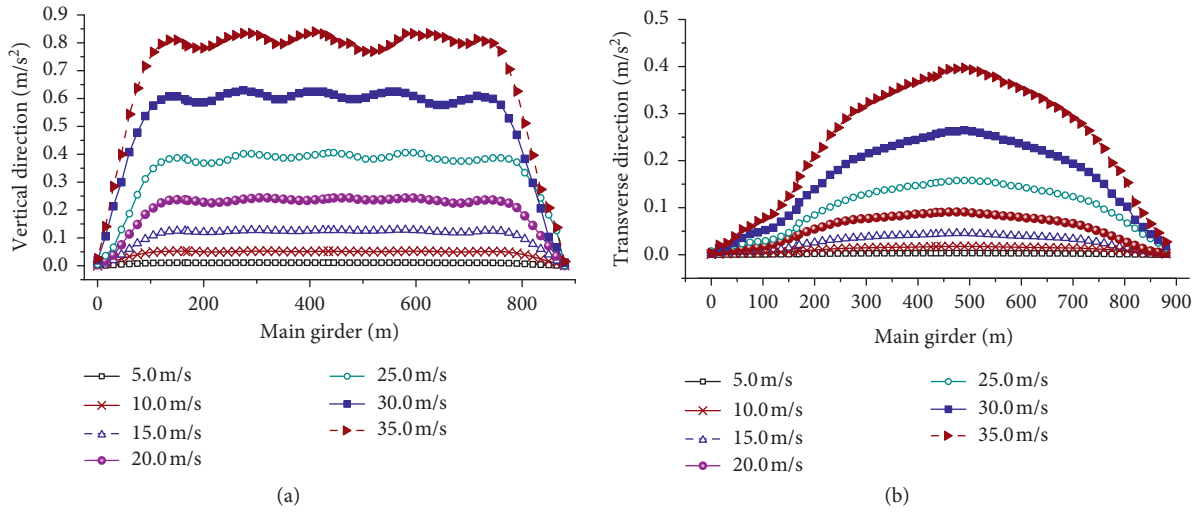

Figure 7: Acceleration along the main girder at different wind velocities: (a) vertical and (b) transverse.

ordinate is the logarithmic coordinate. Main impact frequencies in the vertical direction are mainly concentrated on 0.11 Hz and 0.34 Hz. Main impact frequencies in the transverse direction are mainly concentrated on 0.26 Hz and 0.45 Hz. Accelerations at different positions in Figure 7 are the average accelerations in 600.0 s. In the model of the vehicle-bridge system, force induced by buffeting performance of the bridge is calculated by acceleration, and this force is taken into consideration in the vehicle model. Figure 7 provides results of acceleration along the main girder with seven different wind velocities. Accelerations in vertical and transverse directions increase with increase in wind velocity. Increasing extent of accelerations increase as wind velocity rises, which behaves very

obviously from 1/8 main girder to 7/8 main girder. Under certain assumptions, this can be construed as nonlinear effect of flexible structures. The maximum acceleration is located in the middle of the main girder at different wind velocities. It is speculated that the bridge is a symmetrical structure which is equivalent to a simply supported beam.

2.2. Vehicle Model. Sedan, minibus, microbus, motor bus, van, and container car are taken as research subjects. The safety evaluation model of the vehicle-bridge system with lateral wind is analyzed, and all of vehicle models are calculated according to empty load during the analysis. Basic parameters of vehicles are shown in Table 2.

A mechanical model of the vehicle on the bridge is given in Figure 8. In the mechanical model of the vehicle-bridge system, influence of bridge vibration is taken into consideration with horizontal and vertical inertia forces. Forces acting on the barycenter of the vehicle body and vehicle are analyzed for different vehicle speeds and weather conditions. Force on the vehicle includes lateral aerodynamic force, aerodynamic lift, centrifugal force, and gravity. Also, force on the vehicle could be expressed in the following equations:

$$F_{\text{perp}} = (mg - F_L - F_{bV})\cos\alpha + (F_S + F_I + F_{bH})\sin\alpha, \tag{10}$$

$$F_{\text{para}} = (-mg - F_L - F_{bV})\sin\alpha + (F_S + F_I + F_{bH})\cos\alpha, \tag{11}$$

where F_{perp} and F_{para} are composite forces in the vertical direction and horizontal direction, m is vehicle mass, α is the included angle between the bridge surface and horizontal direction, R is the turning radius of the bridge surface, F_S, F_L, and F_I are aerodynamic forces acting on the vehicle and could be calculated by equations (12)–(14), and F_{bH} and F_{bV} are forces induced by buffeting performance of the bridge and could be calculated by equations (15) and (16).

$$F_S = 0.5\rho U_R^2\left(k_1 c_s\psi + k_2 c_s\psi^2 + k_3 c_s\psi^3\right), \tag{12}$$

$$F_L = 0.5\rho U_R^2 k c_L\psi, \tag{13}$$

$$F_I = \frac{mU_{\text{v}}^2}{R}, \tag{14}$$

$$F_{bH} = ma_{bH}, \tag{15}$$

$$F_{bV} = ma_{bV}, \tag{16}$$

where U_R is the relative wind velocity of the vehicle, and it is given in Figure 8; ρ is the air density; k_1c_s, k_2c_s, and k_3c_s are lateral coefficient parameters; kc_L is the lift coefficient parameter, and aerodynamic coefficient parameters are given in Table 3; ψ is the angle of wind deflection; U_{v} is the speed of the vehicle; and a_{bH} and a_{bV} are the accelerations induced by transverse and vertical buffeting forces, respectively.

3. Accident Types and Criteria

Baker [39] classified the cross wind accidents into three types: rollover accident, rotating accident, and sideslip accident. The criterion of rollover accident is that contact force reduces to zero. The criterion of rotating accident is that value of yaw angle is over 0.2 rad. The criterion of sideslip is that lateral displacement exceeds 0.5 m.

Acceleration of the bridge is introduced into *Baker's* criteria in order to consider response of the bridge. Forces on the vehicle are assumed on the center of vehicle's width and height, and then rollover moment can be expressed in the following equation:

$$M_{\text{rollover}} = \frac{1}{2}\left(HF_{\text{para}} - BF_{\text{perp}}\right), \tag{17}$$

where M_{rollover} is the rollover moment of the vehicle, H is the vehicle's height, m, and B is the vehicle's width, m. When rollover moment equates to a positive value, rollover accident is affirmed. Friction between vehicle and bridge surface is mainly caused by lateral wind load on vehicle, and friction can be expressed in the following equation:

$$F_{\text{f}} = \mu_{\text{s}} F_{\text{para}}. \tag{18}$$

F_{f} is the friction, N. μ_{s} is the friction coefficient, and weather conditions could be reflected by friction coefficient. Dry bridge surface, wet bridge surface, snow bridge surface, and ice bridge surface are taken as 0.7, 0.5, 0.15, and 0.07, respectively, corresponding to wind, rain, snow, and ice weather. When F_{f} is less than F_{para}, rotating accident is affirmed. Sideslip is vehicle's lateral displacement caused by all lateral forces. When the lateral displacement of vehicle reaches 0.5 m, sideslip accident is affirmed. Sideslip can be calculated from the following equation:

$$D_{\text{s}} = \frac{1}{2}\frac{F_{\text{para}}}{m}t^2. \tag{19}$$

D_{s} is the lateral displacement of the vehicle, and t is the reaction time of the diver, and it is determined by wind velocity. When the wind velocity exceeds 15.0 m/s, control frequency of the driver is 2.0 Hz, and hence t is taken as 0.5 s. When the wind velocity is less than 15.0 m/s, control frequency of the driver is 1.0 Hz, and hence t is taken as 1.0 s [40].

In the vehicle-bridge system, dynamic forces on the vehicle components caused by vehicle-bridge interaction during the passage of the vehicle are analyzed individually for different velocities and weather conditions, and the results have been presented. According to judging criteria, safe driving critical values are given by considering the weather effect and bridge response, and data are computed in Matlab software and results are shown in Figure 9.

Figure 9 provides the effect of weather condition including wind, rain, snow, and ice on the vehicle, with the vehicle parameters given in Tables 2 and 3. From Figures 9(a)–9(c), it can be known that rollover accident has the largest limitation of wind velocity at the same vehicle speed. Compared with other types of accidents, rollover accident has the smallest occurring probability in sedan,

Table 2: Basic parameters of vehicles.

Type	Wheel base (m)	Width (m)	Height (m)	Projected area (m^2)	Mass (kg)
Sedan	2.656	1.700	1.423	2.05	1140
Minibus	2.350	1.475	1.895	2.30	965
Microbus	4.290	2.250	2.900	5.55	7100
Motorbus	6.200	2.500	3.700	7.87	12840
Van	2.500	1.800	2.800	4.22	1840
Container car	12.400	2.480	4.290	8.89	17340

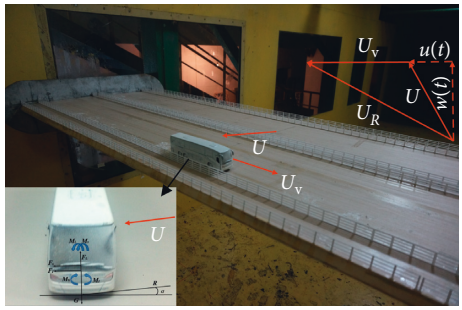

Figure 8: Mechanical model of the vehicle-bridge system.

minibus, and microbus. From Figures 9(d)–9(f), it is found that sideslip accident with dry bridge surface is least impossible to happen on motor bus, van, and container car. The worst weather condition for all types of vehicles is ice and wind weather, and the sideslip accident is most likely to happen on all types of vehicle. Rotating accident is always easier to occur than rollover accident to all types of vehicle with same vehicle speed. Rollover accident has the closest critical value with sideslip accident with wet bridge surface in all vehicles except sedan. When wind velocity is less than 30.0 m/s and vehicle speed is less than 120.0 km/h, minibus and van are easier to stay in an unsafe state.

Results in Figure 9 are taken as training, validation, and testing data in the fully connected neural network (FCN) model. Taking sedan as an example, when the vehicle speed is 80.0 km/h on sunny weather, the rollover accident will happen when the wind speed is over 48.9 m/s. The following is rotating accident when the wind speed is over 43.5 m/s, and sideslip accident when the wind speed is over 40.1 m/s. The input variables are vehicle type, vehicle speed, wind velocity, and weather condition, and the output variable is the probability of four possible car states.

4. Safety Evaluation Model Based on FCN

There are many types of neural networks such as feed-forward back-propagation, radial basis function, recurrent, artificial neural network, and modular neural networks [41–43]. These neural networks vary in structure and information flow, but all have neurons and connection weights. FCN has a strong nonlinear mapping ability and self-adaptive learning, and hence it is widely used in many domains. The nonlinear dynamic system based on FCN has a strong fault tolerance and robustness and function of learning, memorization, and association. Due to this, FCN is very suitable for predicting vibration characteristics of vehicles on bridges. The development of an FCN model involves choice of network variables, determining network structure, and network training-validation-testing procedures. Network variables are first determined by need of the safety evaluation model. The candidate variables are further screened by significant relationship between the input and output variables. The input-output relationships can be examined using model-free or model-based techniques [43, 44].

4.1. Structure and Configuration of Safety Evaluation Model. The vehicle safety evaluation model is based on a FCN, which consists of an input layer and ouput layer with hidden layers. Therefore with vehicle type, vehicle speed, wind velocity, and weather condition as the input vectors after vectorization and normalization, the output value is the predicted probability of four possible car states, including safety, rollover, rotating, and sideslips, respectively. Due to the uncertainty of problem complexity in the design of neural network, a reasonable and usual way is to choose several models with different structure configuration. Some different combinations of dominant superparameter are initialized to search optimal model, such as the depth of network, the number of neurons in each hidden layers, learning rate, batch size, and optimization method. As can be seen in Table 4, two or more options of each superparameter are considered. Also, the schematic architecture of some of all models established in this paper are presented in Figure 10.

These proposed models are all based on the theory of traditional multilayered feed-forward neural network. As the most well-known optimization algorithms in this theoretical field, gradient descent has been shown to be a powerful optimizer for training various neural networks. However, with the number of parameter in optimization objective function increasing, the original gradient descent often shows a poor performance in terms of the convergence speed or searching a global minimum. Thus, to ensure high efficiency of network training, two enhanced gradient descent algorithms are implemented in this paper: *SGD with momentum* [42, 44] and *Adam* [45].

(1) *SGD with Momentum*. Momentum can accelerate the ordinary stochastic gradient descent in the relevant direction and dampens oscillations. It does this by adding a fraction γ of the vector increment of the previous time step to the current vector increment, as shown in equation below. The momentum γ is usually set to 0.9 or other similar value. It can be expressed in the following equations:

Table 3: Aerodynamic coefficient parameters.

Vehicle type	Lift coefficient parameter	Lateral coefficient parameters		
	kc_L	k_1c_s	k_2c_s	k_3c_s
Sedan	0.02	0.047	$-5.130E-04$	$1.675E-06$
Minibus	0.04	0.079	$-2.205E-04$	$-2.820E-06$
Microbus	0.04	0.195	$5.929E-05$	$-1.172E-05$
Motor bus	0.04	0.195	$5.929E-05$	$-1.172E-05$
Van	0.04	0.079	$-2.205E-04$	$-2.820E-06$
Container car	0.04	0.195	$5.929E-05$	$-1.172E-05$

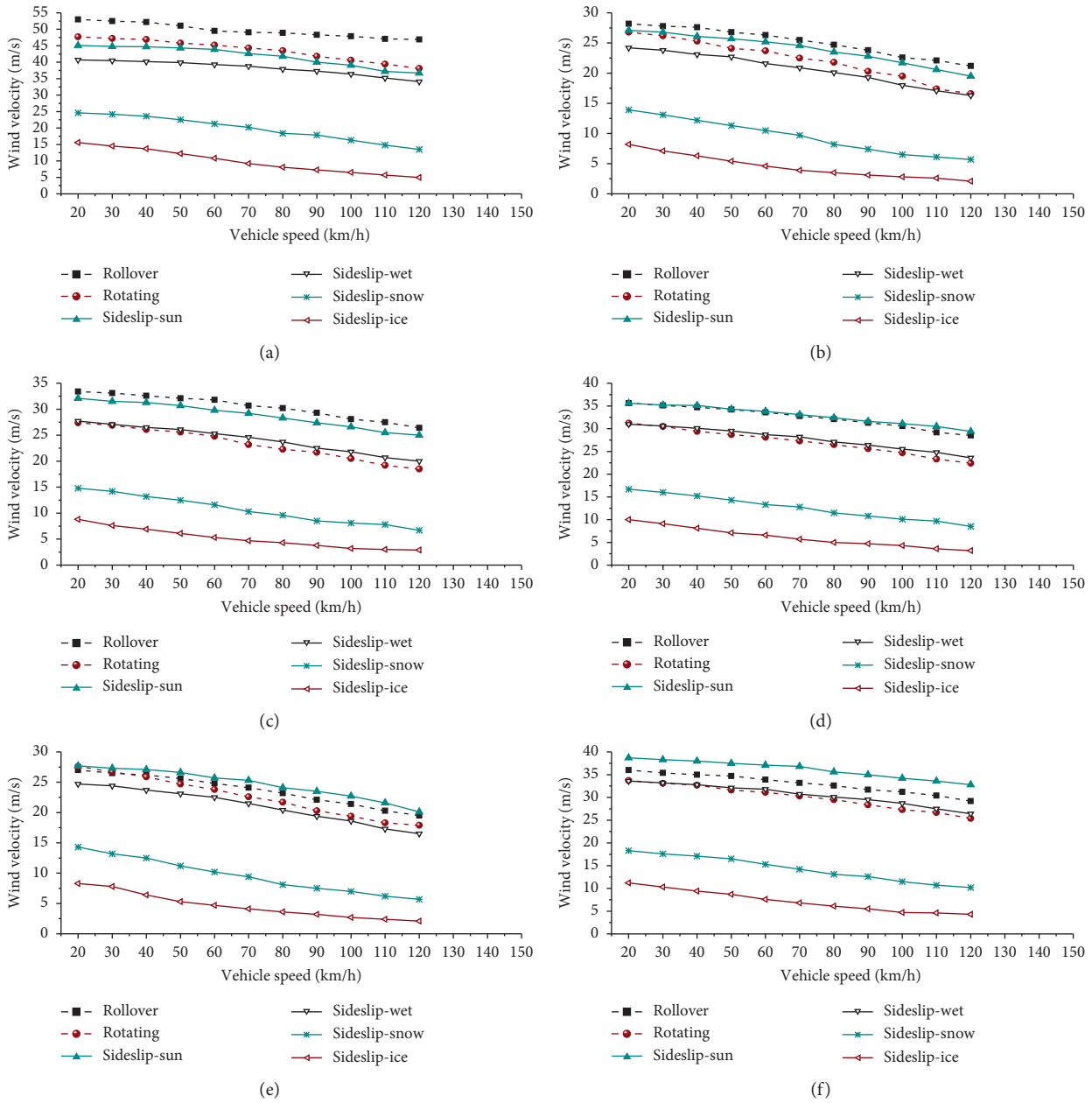

Figure 9: Safe driving critical value of the vehicle-bridge system: (a) sedan, (b) minibus, (c) microbus, (d) motor bus, (e) van, and (f) container car.

Table 4: Optional parameters of models.

Superparameter	Options
Hidden layer	2, 4, 8, 12, 16, 3/3, 7/7, 10/10, 15/15
Initial learning rate	0.05, 0.01
Batch size (per iteration)	100, 250, 500
Activation function	*ReLU*, *LeakyReLU*
Optimization method	*SGD with momentum*, *Adam*

$$v_t = \gamma v_{t-1} + \eta \nabla_\theta J(\theta), \tag{20}$$

$$\theta = \theta - v_t. \tag{21}$$

(2) *Adam*. Adaptive moment estimation is a method that can compute adaptive learning rates for every parameter. *Adam* stores and meanwhile keeps an exponentially decaying average of previous gradients as v_t and m_t, which are estimates of the mean moment and the uncentered variance moment of gradients, repectively. The proposed default values of β_1 and β_2 are usually set to 0.9 and 0.999, respectively. It can be expressed in the following equations:

$$m_t = \beta_1 m_{t-1} + (1 - \beta_1) g_t, \tag{22}$$

$$v_t = \beta_2 v_{t-1} + (1 - \beta_2) g_t^2. \tag{23}$$

In addition to the optimization method, two different types of activation function are adopted including *ReLU* [46] and *LeakyReLU* [47] for parameter analysis. Particularly with a more deeper network being built like in Figure 10(c), a technique called "Dropout" [48, 49] is implemented to prevent overfitting because of the small dataset in this study. The key idea of "Dropout" is to randomly drop some nodes (means breaking the connection between neurons) in each layer during training but make a normal prediction without dropping any units of model when testing the model. It has been confirmed that this trick significantly reduces overfitting and gives major improvements over other regularization methods.

4.2. Training and Evaluation of Safety Evaluation Model. All models built in this paper are based on Pytorch (v1.1), one of the most popular deep learning frameworks currently. Other configuration of computer environment includes Python 3.6, Ubuntu 16.04(OS), and Intel Core i7 7700K(CPU).

In the training stage, a total of 2100 group data calculated from numerical simulation are divided into training, validation, and test sets with 1500, 300, and 300 groups of data, respectively. As shown in Table 4, twenty-nine models are trained with the max-epochs of 100 using training set and validated using validation set in the end of each epoch. During the training process, the max value of validation accuracy and its corresponding epoch number are recorded. When the training of every model is done, the test accuracy of each model can be obtained using the test set. More details of all model training are also presented in Table 4.

The training results show that the final test accuracy of all models has reached more than 90% with the highest and lowest up to 94.983% and 90.97%, respectively. It is indicated that these models all have a good performance on car states prediction. The major difference among models is the convergence velocity, which can be known from the No. Epochs of max validation accuracy in Table 5. For example, when in the 3rd epoch, No. 15 model has reached the maximum validate accuracy. But it was not until the 91st epoch that No. 3 model tended to converge and began to keep stable in the maximum accuracy level. Obviously, a trade-off between model accuracy and training speed is inevitable here.

Considering that there is no great difference between test accuracies, it is reasonable that the less time training process needs to reach the highest precision, the lower model training cost is. Therefore the No. 10 (4-8-4), No. 17 (4-3-3-4), and No. 28 (4-15-15-4) models are selected to do evaluation on the real dataset in the following study. In order to verify the validity of model training, the training process curve of three models with training loss and validation accuracy is shown in Figure 11. From Figure 11, it can be seen that the loss function is on the decline with training epochs increasing and the network loss begin to steadily keep on a very low level from different epochs. At the same time, the time points of max validation accuracy of three models basically agree with No. Epochs (13, 27, 11) in Table 5.

To evaluate the performance of three models on real dataset, the well-trained proposed model is tested with 2000 groups of actual data collected by sensors or other monitoring devices as input. Those actual data include all four types of possible car states with each containing 500 group sets. For analysing the prediction performance of models on each car state separately, the output probability that corresponds to the real label is extracted from the predicted values of four types of labels. Then the deviation between the theoretical probability (or 1.0) and predicted probability was calculated and denoted as predicted score error. With 500 data sets of each type of labels set to be x-axis and predicted score error set to be y-axis, the distribution of prediction errors of three models is shown in Figure 12. Furthermore, a statistical analysis in different prediction error intervals (<0.05, <0.1, <0.15) is presented in Table 6.

Figure 12 shows that the predicted error of three models is largely distributed at a low level even though there are a lot of discrete points above the line $y = 0.4$. But to be more specific, it can be obtained that the concentration of error distribution in the 4-15-15-4 model is higher and the number of discrete points is less than the two other models. Combined with statistics in Table 6, it is indicated that the 4-15-15-4 model occupies a preferable prediction performance on four types of car states from the whole point of view. Moreover, it is noted that the average percentage of data points whose prediction error locates between 0 and 0.05, 0 and 0.10, or 0 and 0.15 has

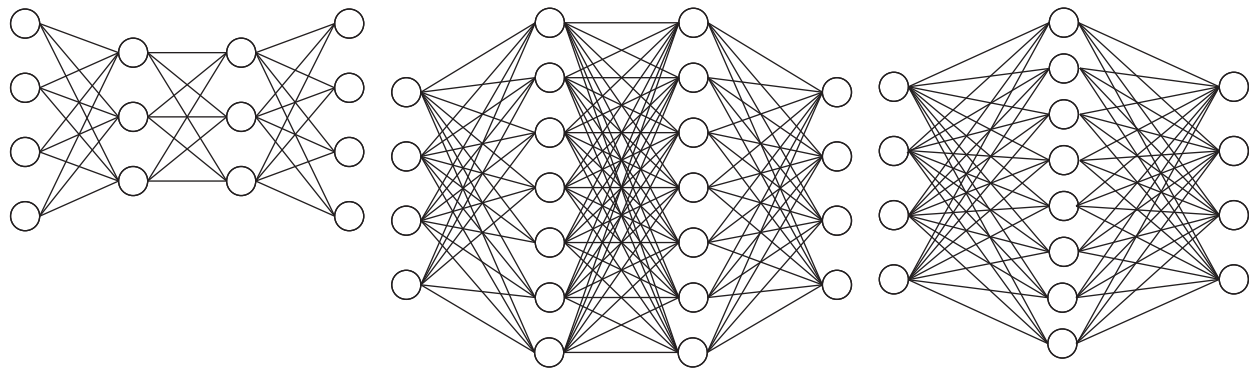

Figure 10: Schematic architecture of FCN. (a) 4-3-3-4. (b) 4-7-7-4. (c) 4-8-4.

Table 5: Details of network training with different superparameter settings.

No.	Hidden layer	Network structure	Initial learning rate	Batch size	Activation function	Optimization method	Max val acc (%)	No. Epochs	Test acc (%)
1	2	4-2-4	0.05	100	ReLU	SGD + momentum	92.64	33	91.304
2	2	4-2-4	0.05	250	ReLU	SGD + momentum	93.31	82	92.642
3	2	4-2-4	0.05	500	ReLU	SGD + momentum	91.64	91	90.97
4	2	4-2-4	0.05	500	LeakyReLU	SGD + momentum	91.30	75	93.98
5	2	4-2-4	0.05	500	LeakyReLU	Adam	92.98	67	91.304
6	2	4-2-4	0.01	500	LeakyReLU	Adam	92.64	82	91.973
7	4	4-4-4	0.05	100	ReLU	SGD + momentum	93.98	43	94.649
8	8	4-8-4	0.05	100	ReLU	SGD + momentum	93.31	10	93.98
9	8	4-8-4	0.05	250	ReLU	SGD + momentum	93.65	14	93.98
10	**8**	**4-8-4**	**0.05**	**500**	**ReLU**	**SGD + momentum**	**93.98**	**13**	**94.649**
11	8	4-8-4	0.05	500	LeakyReLU	SGD + momentum	93.65	21	94.314
12	8	4-8-4	0.05	500	LeakyReLU	Adam	93.65	41	94.649
13	8	4-8-4	0.01	500	LeakyReLU	Adam	93.31	73	94.983
14	12	4-12-4	0.05	100	ReLU	SGD + momentum	94.65	5	93.645
15	16	4-16-4	0.05	100	ReLU	SGD + momentum	93.65	3	93.98
16	3/3	4-3-3-4	0.05	100	ReLU	SGD + momentum	92.98	27	94.314
17	**3/3**	**4-3-3-4**	**0.05**	**250**	**ReLU**	**SGD + momentum**	**92.98**	**27**	**94.649**
18	3/3	4-3-3-4	0.05	500	ReLU	SGD + momentum	93.31	61	92.977
19	3/3	4-3-3-4	0.05	500	LeakyReLU	SGD + momentum	93.65	90	94.314
20	3/3	4-3-3-4	0.05	500	LeakyReLU	Adam	93.31	50	94.983
21	3/3	4-3-3-4	0.01	500	LeakyReLU	Adam	92.31	86	93.311
22	7/7	4-7-7-4	0.05	100	ReLU	SGD + momentum	93.65	36	94.314
23	10/10	4-10-10-4 (Dropout)	0.05	100	ReLU	SGD + momentum	92.98	48	94.983
24	15/15	4-15-15-4 (Dropout)	0.05	100	ReLU	SGD + momentum	93.98	31	94.983
25	15/15	4-15-15-4 (Dropout)	0.05	250	ReLU	SGD + momentum	92.98	11	93.98
26	15/15	4-15-15-4 (Dropout)	0.05	500	ReLU	SGD + momentum	93.31	16	94.314
27	15/15	4-15-15-4 (Dropout)	0.05	500	LeakyReLU	SGD + momentum	93.65	20	94.983
28	**15/15**	**4-15-15-4 (Dropout)**	**0.05**	**500**	**LeakyReLU**	**Adam**	**94.98**	**11**	**94.983**
29	15/15	4-15-15-4 (Dropout)	0.01	500	LeakyReLU	Adam	91.97	35	93.645

been more than 90%. Hence, for four types of given labels, all three models have a better prediction ability to the data labelled with slideslip. In summary, although there is some difference between models or labelled data, over 83.0% of model predictions can guarantee more than 85.0% confidence for the real labels.

The analysis result above indicates that the safety prediction model of car states on the bridge has certain

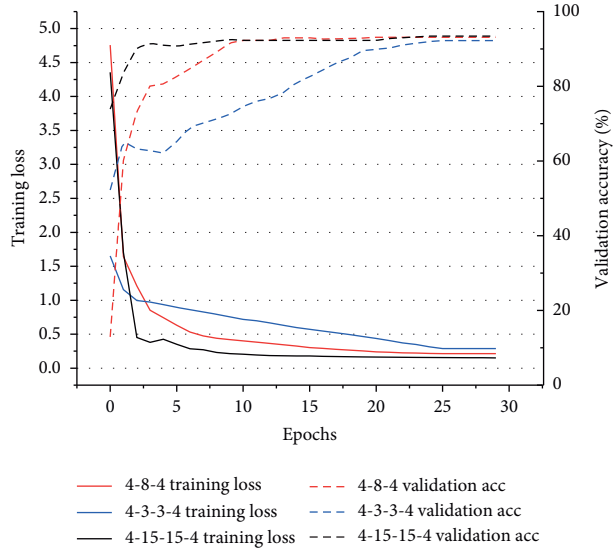

Figure 11: The training loss curve.

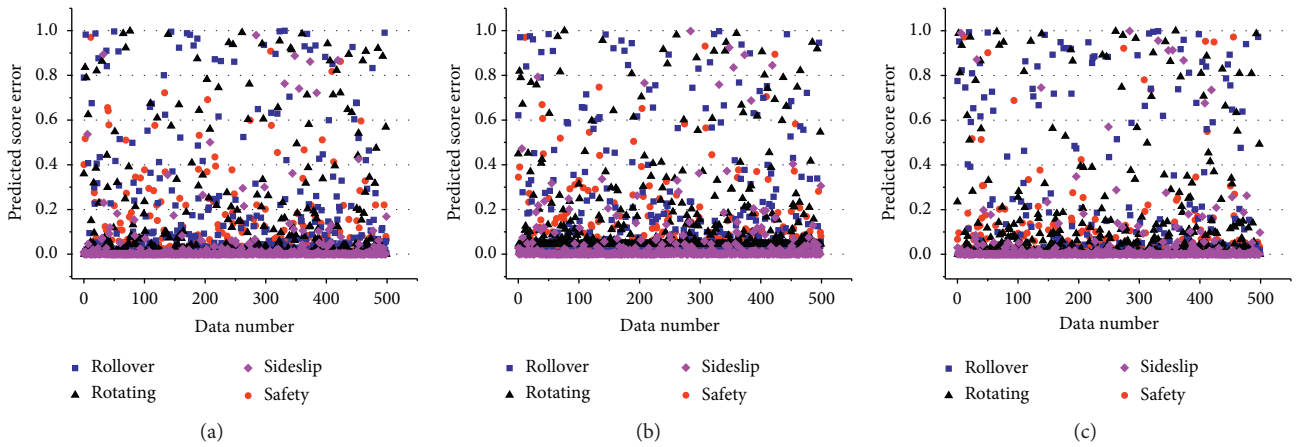

Figure 12: Prediction errors of models. (a) 4-8-4. (b) 4-3-3-4. (c) 4-15-15-4.

Table 6: Statistical analysis of predicted score error.

Car state	Model	Error intervals		
		<0.05 (%)	<0.1 (%)	<0.15 (%)
Safety	4-8-4	0.74 (370)*	0.826 (413)	0.874 (437)
	4-3-3-4	0.72 (360)	0.828 (414)	0.872 (436)
	4-15-15-4	**0.804 (402)**	**0.886 (443)**	**0.922 (461)**
Rollover	4-8-4	0.644 (322)	0.744 (372)	0.782 (391)
	4-3-3-4	0.638 (319)	0.722 (361)	0.762 (381)
	4-15-15-4	**0.744 (372)**	**0.79 (395)**	**0.814 (407)**
Rotating	4-8-4	**0.706 (353)**	0.772 (386)	0.806 (403)
	4-3-3-4	0.564 (282)	0.714 (357)	0.772 (386)
	4-15-15-4	0.664 (332)	**0.776 (388)**	**0.83 (415)**
Sideslip	4-8-4	0.91 (455)	**0.94 (470)**	**0.956 (478)**
	4-3-3-4	0.878 (439)	0.916 (458)	0.938 (469)
	4-15-15-4	**0.912 (456)**	0.938 (469)	0.952 (476)
(Total)	4-8-5	0.75 (1500)	0.82 (1641)	0.8545 (1709)
	4-3-3-5	0.7 (1400)	0.795 (1590)	0.836 (1672)
	4-15-15-5	**0.781 (1562)**	**0.8475 (1695)**	**0.8795 (1759)**

*370 in bracket indicates the number of corresponding data.

credibility and vehicle safety evaluation model based on FCN can improve computational efficiency and prediction accuracy. It provides a kind of utility for traffic control on the bridge and reduces the probability of vehicle accidents on the bridge.

5. Conclusions

This research presents a vehicle safety evaluation model based on FCN. The interaction between the bridge and vehicle and the weather effect on the vehicle-bridge system have been taken into account. This paper contributes development of neural network models for performing effective safety prediction of vehicles passing on the bridge.

Firstly, dynamic responses of the bridge under different wind excitations are computed by the finite element model. The maximum acceleration is located in the middle of the main girder at different wind velocities. Accelerations in vertical and transverse directions increase with increase in wind velocity, and increasing extent of accelerations increase as wind velocity rises. The bridge model and vehicle model are established by considering the severe weather effect.

Second, accident types and criteria are given including interaction between the bridge and vehicle. Results of safe driving critical value are calculated and given. The worst weather condition for vehicles is ice and wind weather, and the sideslip accident is most likely to happen on all types of vehicle.

Finally, twenty-nine safety evaluation models based on FCN are established, and models have been compared and analyzed by hidden layer, initial learning rate, batch size, activation function, and optimization method. It is proved that the safety prediction model of car states on the bridge has certain credibility and the vehicle safety evaluation model based on FCN can improve computational efficiency and prediction accuracy. The proposed 4-15-15-4 model, taking into account severe weather including wind, rain, snow, and ice, is a full-scale analysis tool and can be very useful for setting the travelling speed limit or making operational decisions for severe weather.

Data Availability

The data used to support the findings of this study are available from the corresponding author upon request.

Conflicts of Interest

The authors declare that they have no conflicts of interest.

Acknowledgments

This work was financially supported by the National Natural Science Foundation of China (51608074) and Fundamental Research Funds for the Central Universities (2019CDXYTM0032, 2019CDQYTM028, and 106112017CDJXY200009).

References

[1] C. S. Cai, J. Hu, S. Chen, Y. Han, W. Zhang, and X. Kong, "A coupled wind-vehicle-bridge system and its applications: a review," *Wind and Structures*, vol. 20, no. 2, pp. 117–142, 2015.

[2] Y. Han, S. Liu, C. S. Cai, J. Zhang, S. Chen, and X. He, "The influence of vehicles on the flutter stability of a long-span suspension bridge," *Wind and Structures*, vol. 20, no. 2, pp. 275–292, 2015.

[3] Y. Yang, Z. L. Liang, W. Bo, and L. Xin, "Vehicle effect on vortex-induced vibration of flat steel box girder," *The Open Civil Engineering Journal*, vol. 10, no. 1, pp. 12–24, 2016.

[4] K. L. Lu, W. G. Zhang, and Y. Liu, "Container vehicle-truss bridge coupled vibration analysis and structural safety assessment under stochastic excitation," *Journal of Vibroengineering*, vol. 16, no. 6, pp. 3122–3136, 2014.

[5] A. Camara and A. M. Ruiz-Teran, "Multi-mode traffic-induced vibrations in composite ladder-deck bridges under heavy moving vehicles," *Journal of Sound and Vibration*, vol. 355, pp. 264–283, 2015.

[6] W. Wang, W. Yan, L. Deng, and H. Kang, "Dynamic analysis of a cable-stayed concrete-filled steel tube arch bridge under vehicle loading," *Journal of Bridge Engineering*, vol. 20, no. 5, Article ID 04014082, 2015.

[7] M. M. S. Cheung and B. Y. B. Chan, "Performance and operational allowable speed limit for vehicles on cable stayed bridges," *Bridge Structures*, vol. 6, no. 2, pp. 3–24, 2010.

[8] M. M. S. Cheung and B. Y. B. Chan, "Operational requirements for long-span bridges under strong wind events," *Journal of Bridge Engineering*, vol. 15, no. 2, pp. 131–143, 2010.

[9] Y. Liu, X. Yin, L. Deng, and C. S. Cai, "Ride comfort of the bridge-traffic-wind coupled system considering bridge surface deterioration," *Wind and Structures*, vol. 23, no. 1, pp. 19–43, 2016.

[10] X. Yin, Y. Liu, and S. R. Chen, "Assessment of ride safety based on the wind-traffic-pavement-bridge coupled vibration," *Wind and Structures*, vol. 24, no. 3, pp. 287–306, 2017.

[11] Y. Zhou and S. Chen, "Vehicle ride comfort analysis with whole-body vibration on long-span bridges subjected to crosswind," *Journal of Wind Engineering and Industrial Aerodynamics*, vol. 155, pp. 126–140, 2016.

[12] O. Mohammed and A. González, "Static and dynamic moments for any plane within a straight solid slab bridge caused by the crossing of a truck," *Engineering Structures*, vol. 150, pp. 465–480, 2017.

[13] S. Zhou, G. Song, Z. Ren, and B. Wen, "Nonlinear dynamic analysis of a parametrically excited vehicle-bridge interaction system," *Nonlinear Dynamics*, vol. 88, no. 3, pp. 2139–2159, 2017.

[14] M. A. Koç and İ. Esen, "Modelling and analysis of vehicle-structure-road coupled interaction considering structural flexibility, vehicle parameters and road roughness," *Journal of Mechanical Science and Technology*, vol. 31, no. 5, pp. 2057–2074, 2017.

[15] J. Melcer, "Dynamic response of a bridge due to moving loads," *Journal of Vibration Engineering & Technologies*, vol. 3, no. 2, pp. 199–209, 2015.

[16] Y. L. Xu and W. H. Guo, "Dynamic analysis of coupled road vehicle and cable-stayed bridge systems under turbulent wind," *Engineering Structures*, vol. 25, no. 4, pp. 473–486, 2003.

[17] C. S. Cai and S. R. Chen, "Framework of vehicle–bridge–wind dynamic analysis," *Journal of Wind Engineering and Industrial Aerodynamics*, vol. 92, no. 7-8, pp. 579–607, 2004.

[18] L. Deng, R. Cao, W. Wang, and X. Yin, "A multi-point tire model for studying bridge–vehicle coupled vibration," *International Journal of Structural Stability and Dynamics*, vol. 16, no. 8, Article ID 1550047, 2016.

[19] Q. Gao, Z. Wang, B. Guo, and C. Chen, "Dynamic responses of simply supported girder bridges to moving vehicular loads based on mathematical methods," *Mathematical Problems in Engineering*, vol. 2014, Article ID 514872, 22 pages, 2014.

[20] W. H. Guo and Y. L. Xu, "Fully computerized approach to study cable-stayed bridge-vehicle interaction," *Journal of Sound and Vibration*, vol. 248, no. 4, pp. 745–761, 2001.

[21] S. R. Chen and J. Wu, "Dynamic performance simulation of long-span bridge under combined loads of stochastic traffic and wind," *Journal of Bridge Engineering*, vol. 15, no. 3, pp. 219–230, 2010.

[22] D. Rocchi, L. Rosa, E. Sabbioni, M. Sbrosi, and M. Belloli, "A numerical-experimental methodology for simulating the aerodynamic forces acting on a moving vehicle passing through the wake of a bridge tower under cross wind," *Journal of Wind Engineering and Industrial Aerodynamics*, vol. 104–106, pp. 256–265, 2012.

[23] Q. Zou, L. Deng, T. Guo, and X. Yin, "Comparative study of different numerical models for vehicle–bridge interaction analysis," *International Journal of Structural Stability and Dynamics*, vol. 16, no. 9, Article ID 1550057, 2016.

[24] T. Argentini, E. Ozkan, D. Rocchi, L. Rosa, and A. Zasso, "Cross-wind effects on a vehicle crossing the wake of a bridge pylon," *Journal of Wind Engineering and Industrial Aerodynamics*, vol. 99, no. 6-7, pp. 734–740, 2011.

[25] H. Kozmar, K. Butler, and A. Kareem, "Downslope gusty wind loading of vehicles on bridges," *Journal of Bridge Engineering*, vol. 20, no. 11, Article ID 04015008, 2015.

[26] M. Suzuki and Y. Hibino, "Field tests and wind tunnel tests on aerodynamic characteristics of train/vehicles under cross-winds," *Quarterly Report of RTRI*, vol. 57, no. 1, pp. 55–60, 2016.

[27] H. Xiang, Y. Li, S. Chen, and C. Li, "A wind tunnel test method on aerodynamic characteristics of moving vehicles under crosswinds," *Journal of Wind Engineering and Industrial Aerodynamics*, vol. 163, pp. 15–23, 2017.

[28] L. Ma, X. Chen, J. Wu, and W. Han, "Aerodynamic interference mechanism of moving vehicles on a bridge deck in crosswind environment," *Journal of Bridge Engineering*, vol. 23, no. 4, Article ID 04018011, 2018.

[29] S.-J. Kim, C.-H. Yoo, and H.-K. Kim, "Vulnerability assessment for the hazards of crosswinds when vehicles cross a bridge deck," *Journal of Wind Engineering and Industrial Aerodynamics*, vol. 156, pp. 62–71, 2016.

[30] L. Ma, D. Zhou, W. Han, J. Wu, and J. Liu, "Transient aerodynamic forces of a vehicle passing through a bridge tower's wake region in crosswind environment," *Wind and Structures*, vol. 22, no. 2, pp. 211–234, 2016.

[31] S. Stoyanoff, P. O. Dallaire, T. Zoli, and G. Daly, "Vehicle roll-over stability in strong winds on long-span bridges," *Bridge Structures*, vol. 11, no. 4, pp. 149–162, 2016.

[32] S. Pospíšil, A. Buljac, H. Kozmar, S. Kuznetsov, M. Macháček, and R. Král, "Influence of stationary vehicles on bridge aerodynamic and aeroelastic coefficients," *Journal of Bridge Engineering*, vol. 22, no. 4, Article ID 05016012, 2017.

[33] M. Wu, Y. Li, and N. Chen, "The impact of artificial discrete simulation of wind field on vehicle running performance," *Wind and Structures*, vol. 20, no. 2, pp. 169–189, 2015.

[34] L.-B. Wang and P.-W. Jiang, "Numerical computation for vibration characteristics of long-span bridges with considering vehicle-wind coupling excitations based on finite element and neural network models," *Journal of Vibroengineering*, vol. 19, no. 3, pp. 2106–2125, 2017.

[35] F.-H. Dong, "Virtual reality research on vibration characteristics of long-span bridges with considering vehicle and wind loads based on neural networks and finite element method," *Neural Computing and Applications*, vol. 29, no. 5, pp. 1303–1309, 2018.

[36] Y. Gang, Y. Yang, F. Wei, and W. Qin, "Buffeting performance of long-span suspension bridge based on measured wind data in a mountainous region," *Journal of Vibroengineering*, vol. 20, no. 1, pp. 621–635, 2018.

[37] G. Yao, Y. Yang, W. Bo, L. Lianjie, and Z. Liangliang, "Aerodynamic admittance influence on buffeting performance of suspension bridge with streamlined deck," *Journal of Vibroengineering*, vol. 21, no. 1, pp. 198–214, 2019.

[38] C. J. Baker, "A simplified analysis of various types of wind-induced road vehicle accidents," *Journal of Wind Engineering and Industrial Aerodynamics*, vol. 22, no. 1, pp. 69–85, 1986.

[39] G. Yao, F. Wei, Y. Yang, and Y. Sun, "Deep-Learning based bughole detection for concrete surface image," *Advances in Civil Engineering*, vol. 2019, Article ID 8582963, 12 pages, 2019.

[40] Y. J. Ge, "Traffic wind environment and improvement measures," *Wind Resistance of Long Span Suspension Bridges*, vol. 11, 2011.

[41] D. John, H. Elad, and S. Yoram, "Adaptive subgradient methods for online learning and stochastic optimization," *Journal of Machine Learning Research*, vol. 12, pp. 2121–2159, 2011.

[42] S. Ruder, "An overview of gradient descent optimization algorithms," 2016, https://arxiv.org/abs/1609.04747.

[43] N. Qian, "On the momentum term in gradient descent learning algorithms," *Neural Networks*, vol. 12, no. 1, pp. 145–151, 1999.

[44] S. Ioffe and S. Christian, "Batch normalization: accelerating deep network training by reducing internal covariate shift," 2015, https://arxiv.org/abs/1502.03167.

[45] D. P. Kingma and J. Ba, "Adam: a method for stochastic optimization," 2014, https://arxiv.org/abs/1412.6980.

[46] H. Kaiming, Z. Xiangyu, R. Shaoqing, and S. Jian, "Delving deep into rectifiers: surpassing human-level performance on imagenet classification," 2015, https://arxiv.org/abs/1502.01852.

[47] X. Bing, W. Naiyan, C. Tianqi, and M. Li, "Empirical evaluation of rectified activations in convolution network," 2015, https://arxiv.org/abs/1505.00853.

[48] N. Srivastava, G. E. Hinton, and A. Krizhevsky, "Dropout: a simple way to prevent neural networks from overfitting," *The Journal of Machine Learning Research*, vol. 15, no. 1, pp. 1929–1958, 2014.

[49] G. E. Hinton, N. Srivastava, A. Krizhevsky, I. Sutskever, and R. R. Salakhutdinov, "Improving neural networks by preventing co-adaptation of feature detectors," 2012, https://arxiv.org/abs/1207.0580.